J Solid State Electrochem (2012) 16:3363–3370
DOI 10.1007/s10008-012-1783-7

ORIGINAL PAPER

Scanning electrochemical microscopy and video microscopy investigations of Tiron-mediated polypyrrole nucleation on AA2024-T3

Mark B. Jensen · Jake M. Karels · Patrick J. Cool · Audrey F. Guerard · Dennis E. Tallman

Received: 9 April 2012 / Revised: 13 May 2012 / Accepted: 18 May 2012 / Published online: 3 June 2012

Abstract Scanning electrochemical microscopy (SECM) and video microscopy have been used to examine the mediated electrodeposition of polypyrrole on AA2024-T3. Of particular interest is the role of surface heterogeneity (namely, copper-rich secondary phase particles) on electrodeposition mediated by 4,5-dihydroxy-1,3-benzenedisulfonic acid (Tiron). SECM shows that polymer nucleation occurs exclusively on the aluminum matrix of the alloy. Video microscopy shows this to be true on a model alloy (a pure Al substrate with an embedded Cu wire) as well, and also suggests that polymer growth is directional toward the copper-rich sites in the absence of sulfate in the deposition solution. A model is presented in which polymer deposition on the copper-rich sites is inhibited either by $CuSO_4$-induced passivation or by the loss of mediator due to Cu–Tiron complex formation.

Keywords Scanning electrochemical microscopy · Polypyrrole · Corrosion · Aluminum alloy

Introduction

Conducting polymers continue to be of interest as possible alternatives to chromium-containing anticorrosion coatings for active metals and metal alloys due to their potential for altering the corrosion behavior of these surfaces through electronic, chemical, and/or electrochemical interactions [1]. These polymer coatings are often deposited electrochemically using potentiostatic, potentiodynamic, or galvanostatic control since these methods offer accurate control of polymerization rate and polymer thickness, and localize the polymerization at the electrode (substrate) surface. For active metals, the high overpotential required for anodic electrodeposition often results in concomitant formation of an electrically insulating surface oxide layer on the underlying metal, producing a non-uniform, weakly adherent polymer film [1]. This high overpotential can be avoided with the use of an appropriate electrochemical mediator [2]. The oxidation of the mediator is thermodynamically less favorable than oxidation of the monomer, but the potential required for oxidation of the mediator at the substrate is lower due to the absence of the kinetic barriers associated with monomer oxidation. The oxidized mediator subsequently oxidizes the monomer, resulting in polymerization and deposition of the conducting polymer film and regeneration of the mediator back to its reduced form.

It has been demonstrated that the potential required for galvanostatic deposition of polypyrrole on aluminum and aluminum alloys can be decreased by up to 500 mV with the use of 4,5-dihydroxy-1,3-benzenedisulfonic acid (also known as Tiron) as the electrochemical mediator, with deposition proceeding at approximately 100 % current efficiency [3–7]. Both the hydroxyl and sulfonate groups of Tiron have been shown to be important to the overall mediation process [4]. The hydroxyl groups impart electroactivity that provides the electrochemical mediation as described above, while the negatively charged sulfonate groups play a surfactant-like role in facilitating interaction of the hydrophobic pyrrole monomer with the Al alloy surface that is positively charged below the isoelectric pH of 7.2 [8].

M. B. Jensen (✉) · J. M. Karels · P. J. Cool · A. F. Guerard
Department of Chemistry, Concordia College,
Moorhead, MN 56562, USA
e-mail: jensen@cord.edu

D. E. Tallman
Department of Coatings and Polymeric Materials and Department of Chemistry and Biochemistry, North Dakota State University,
Fargo, ND 58108, USA

Indeed, the ability of Tiron to adsorb onto alumina surfaces has been demonstrated previously [9, 10].

The formation of copper-rich intermetallics (or secondary phase particles) in aluminum alloys is necessary to provide the strength required of these materials in many industrial applications [11]. However, it is these copper-rich inclusions that greatly exacerbate the tendency of these alloys to undergo galvanic corrosion, with the Cu-rich inclusions serving as sites for oxygen reduction [11]. Scanning electrochemical microscopy (SECM) has proven to be a powerful tool in determining local variations in electrochemical activity on an electrode surface [12]. Indeed, previous SECM studies from our laboratory have shown that the fastest electron transfer (both oxidation and reduction) for hydroxybenzene compounds at the AA2024-T3 surface occurs at these Cu-rich sites [13, 14]. In this investigation, we turn our attention to the role these secondary particles play in the electrodeposition of polypyrrole, specifically in the nucleation phase.

SECM has found application in a number of conducting polymer studies, including investigations of the potential dependence of the conductivity of a polypyrrole film [15], ion transport and electron transfer at polypyrrole films [16], cation ejection from a styrene-methacrylic acid block copolymer micelle-doped polypyrrole film [17], micropatterned deposition and/or imaging of conducting polymers and conducting polymer composites on inert metals [18–24], and the redox properties of thin films of poly(3,4-ethylenedioxythiophene) [25], and polyaniline [26] on insulating substrates. The purpose of the present study is to use SECM to determine the effect of Cu-rich intermetallic particles on polymer nucleation during the Tiron-mediated electrodeposition of polypyrrole on AA2024-T3. We have used SECM to identify sites of initial polypyrrole nucleation and growth on AA2024-T3, and then compared these locations with those of Cu-rich sites imaged in separate SECM experiments and confirmed with scanning electron microscopy/energy dispersive X-ray analysis (SEM/EDX). These results were compared to those obtained from video microscopy synchronized with potentiodynamic scanning during mediated polypyrrole electrodeposition on a model alloy consisting of a pure Al substrate with an embedded Cu wire. Both SECM and video microscopy clearly show that polymer nucleation is inhibited at Cu-rich sites, resulting in nucleation occurring exclusively on the Al matrix.

Experimental

Materials and sample preparation Reagent grade pyrrole (freshly distilled before use) and Tiron were obtained from Aldrich. Sodium sulfate (Alfa Aesar), hydroquinone (MCB), and potassium ferricyanide (Mallinckrodt) were reagent grade and used as received. Panels of AA2024-T3 were obtained from Q-Panel, and pure Al (99.99%) panels were purchased from Alpha Aesar. Model alloy samples were prepared by embedding a 1-mm diameter Cu wire in pure Al substrate and polishing to flatness to form a small Cu island surrounded by Al. Samples were cut into sizes appropriate for the SECM cell, sanded with 600-grit silicon carbide, rinsed with hexane, and dried in air. A commercial engraver (Gravograph) was used to cut a 2×2 mm square position marker into samples to be used for both SECM and SEM/EDX analysis. Sparging to remove oxygen was deemed unnecessary in the SECM and video microscopy experiments.

Instrumentation SECM experiments were performed with a CHI900B Scanning Electrochemical Microscope (CH Instruments) utilizing a 10-μm Pt microelectrode probe, Pt counter electrode, and a saturated Ag/AgCl reference electrode. The Teflon SECM cell was constructed with one hole through the cell in the center and a second larger concentric hole countersunk from the top to a depth matching the height of the Q-panel samples. A mechanical punch was used to cut these samples from panels to the same diameter as the opening in the cell such that the sample surface is flush with the surface of the cell. Electrical contact between the sample and potentiostat was made through the hole in the middle of the cell with a wire attached to the back of the sample with conductive epoxy, and the sample was secured to the bottom of the cell with tape to prevent leakage of solution. Two tapped holes in the cell, one on either side of the sample, were fitted with Tygon tubing connected to a syringe to allow for efficient removal and replacement of solution with no disturbance of the SECM tip position, an important point when attempting to image the same portion of the sample surface both before and after polymer deposition.

SECM probe heights for imaging were set using probe approach curves, with either HQ or ferricyanide as the mediator. The probe potential was set to either oxidize (hydroquinone) or reduce (ferricyanide) the mediator, and the probe current was measured while moving toward the substrate. The approach was stopped when the current reached 80 % of its original value. The variable and dynamic nature of the AA2024-T3 surface makes accurate height determinations from theoretical fits difficult, but the probe height was estimated at 2–5 μm for all images. SECM images were obtained by scanning 80×80 μm areas of the substrate with 1 μm steps at 16.67 ms per step, resulting in scan times of approximately 2 min per image.

Video microscopy experiments were conducted using the SECM cell. A substrate was prepared and positioned in the cell as described above. The cell was filled with the appropriate deposition solution and a Sony SSC-DC393 video

camera was positioned perpendicular to the cell and focused onto the substrate to show an area approximately 1.3× 1.0 mm. Video images were captured using a National Instruments PCI-1411 color frame grabber. Potentiodynamic electrodeposition was initiated using the CHI900B potentiostat and LabVIEW-generated software was employed to synchronously record substrate current and potential values from the cell along with corresponding snapshots of the substrate surface from the video camera. Time-correlated data points (current and potential) and images were collected at a rate of approximately seven per second. LabVIEW software could then be used to replay the entire experiment to generate compressed movie files or select individual representative images for analysis and/or display.

Samples for SEM/EDX analysis were removed from the SECM cell after imaging, rinsed with water, and placed on aluminum mounts using silver paint. Images were obtained using a JEOL JSM-6490LV Scanning Electron Microscope (JEOL USA, Inc., Peabody, MA, USA). X-ray information was obtained via a Thermo Nanotrace Energy Dispersive X-ray detector with NSS-300e acquisition engine.

Results and discussion

SECM imaging of polymer nucleation sites The electrodeposition of polypyrrole on the alloy surface was carried out potentiodynamically in the SECM cell from a deposition solution consisting of pyrrole (monomer), Tiron (mediator), sodium sulfate (supporting electrolyte), and sulfuric acid (0.001 M). Sodium sulfate is commonly used in the electropolymerization of pyrrole on aluminum as it is known to give a porous-type Al_2O_3 structure that enhances electrical contact between the polymer and the bare aluminum [27, 28], and previous studies have also shown that the optimum Tiron-mediated polypyrrole films on AA2024-T3 are formed at pH 2–3 [6]. Following the initiation of electrodeposition, polymer nucleation sites were identified with SECM in tip generation–substrate collection (TG/SC) mode using ferricyanide as the SECM mediator. In these experiments, ferricyanide is reduced to ferrocyanide at the tip electrode to produce a steady-state tip current. Ferrocyanide at the substrate surface may then be oxidized back to ferricyanide at conductive polypyrrole sites, leading to enhanced tip current due to recycling of the mediator (positive feedback). This behavior would not be observed on the oxide-covered aluminum matrix, as we have previously demonstrated that oxidative activity on the matrix is observed only at very high anodic potentials (≥2 V) [14]. Therefore, areas of the substrate that result in an enhanced cathodic feedback current at the SECM tip should correspond to polypyrrole nucleation sites.

Evidence for the validity of this approach is provided by the results of cyclic voltammetry experiments shown in Fig. 1. The gray curve in Fig. 1 shows the reversible voltammogram ($E^{\circ\prime}$=0.226 V) obtained from ferricyanide at a Pt disk electrode in 0.01 M $Fe(CN)_6^{3-}$/1.0 M Na_2SO_4. The three black curves show voltammograms acquired from an AA2024-T3 substrate in this same solution following various levels of potentiodynamic polymer deposition. The dotted black curve corresponds to bare AA2024-T3 with no polymer. No activity is seen in this case, consistent with very sluggish electron transfer at the (mainly) aluminum oxide surface. The dashed black curve was obtained following deposition of less than a full layer (~50 % surface coverage) of polypyrrole. Here, a quasi-reversible redox couple appears ($E^{\circ\prime}$=0.288 V) that we attribute to ferricyanide reduction/oxidation occurring on the deposited polypyrrole. The solid black curve shows the results following deposition of a full polymer layer. A second couple is now clearly evident with $E^{\circ\prime}$=−0.068 V, which we attribute to oxidation/reduction of polypyrrole. These results demonstrate that ferricyanide is reduced at the Pt SECM tip electrode at potentials less than 0.15 V, while potentials greater than 0.4 V are required for oxidation of ferrocyanide on electrodeposited polypyrrole. The substrate should be maintained at potentials greater than 0.1 V to maintain polypyrrole in its oxidized form. In SECM experiments designed to determine polypyrrole nucleation sites, we have chosen a Pt tip potential of 0.0 V to reduce ferricyanide, and a polypyrrole/AA2024-T3 substrate potential of 0.6 V to oxidize ferrocyanide and maintain the oxidized form of the polymer.

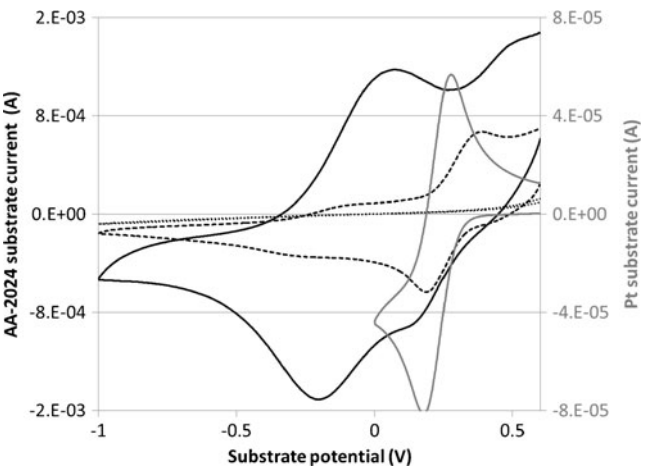

Fig. 1 Cyclic voltammograms of 0.01 M $K_3Fe(CN)_6$ in 1 M Na_2SO_4 on various substrates. *Black* (*left y-axis*) AA2024-T3 following potentiodynamic polypyrrole electrodeposition of full polymer layer (*solid*), partial polymer layer (*dashed*), no polymer (*dotted*). Polymer deposition solution: 0.1 M pyrrole, 0.1 M Tiron, 1 M Na_2SO_4, and 0.001 M H_2SO_4; deposition scan rate, 10 mV/s; CV scan rate, 100 mV/s. *Gray* (*right y-axis*) Pt disk electrode (1.6 mm diameter) at 150 mV/s

Figure 2 shows the results of combined SECM/EDX experiments carried out on an 80×80 μm section of AA2024-T3 to determine both cathodically active Cu-rich sites on the bare alloy, as well as anodically active polypyrrole following initiation of electrodeposition. The areas in Fig. 2a and b showing high anodic tip current correspond to copper sites, most likely AlCuFeMn or Al_2CuMg (S-phase) intermetallic particles. (Figure 2a and b are identical except for the circles added around the active spots in Fig. 2b as a common reference for the other images in the figure.) Regions of rather pure Cu are also known to form on this dynamic alloy surface, the result of surface preparation [29] and/or dealloying of S-phase particles in acidic solution, often with redistribution of Cu across the alloy surface [30]. The image of Fig. 2a,b was obtained in TG/SC mode using hydroquinone as the SECM mediator. Our choice of hydroquinone stems from our interest in the electron transfer reactions of hydroxybenzene compounds that mediate electrodeposition of polymer (e.g., Tiron) on the alloy surface. (Tiron proved to be an unsuitable mediator due to the lack of a steady-state anodic current presumably due to self-oligomerization [14].) The tip potential in Fig. 2a, b was held at +1.2 V to oxidize the hydroquinone to benzoquinone and produce a steady-state current. The substrate was held at −0.8 V (the open-circuit potential under these conditions), to reduce benzoquinone back to hydroquinone which may then be re-oxidized at the tip resulting in positive feedback. The active areas in Fig. 2a, b represent areas of high cathodic substrate activity and correspond very well to the bright areas of the Cu EDX map shown in Fig. 2c, consistent with our previous conclusion that cathodically active sites on AA2024-T3 represent Cu-rich inclusions in the alloy [14].

Following the acquisition of the image in Fig. 2a, b, the tip was raised and the hydroquinone solution was removed from the cell. The cell was rinsed several times with DI water and a deposition solution of 0.1 M pyrrole, 0.1 M Tiron, 1.0 M Na_2SO_4, and 0.001 M H_2SO_4 was added to the cell. While visually monitoring the substrate with the video camera, the substrate potential was increased at 10 mV/s from 0.0 V until polymer nucleation was visible (0.817 V), at which point the potential sweep was terminated. The deposition solution was then rinsed from the cell and replaced with 0.01 M $K_3Fe(CN)_6$ in 1.0 M Na_2SO_4. The SECM tip was lowered back toward the substrate and the same 80×80 μm area was imaged again using the parameters described above for determination of polymer sites, the

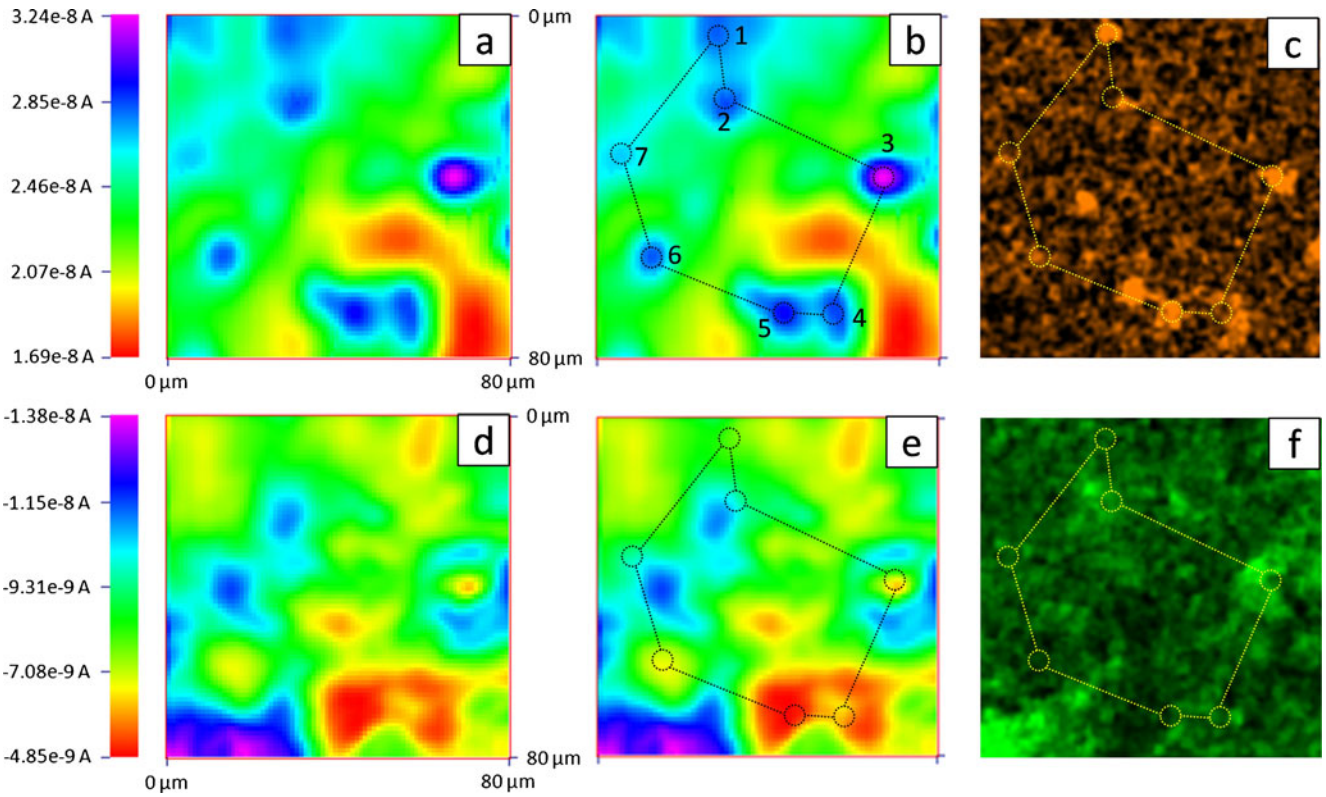

Fig. 2 **a** SECM image of AA2024-T3 obtained with a 10 μm Pt probe electrode in 0.01 M hydroquinone, 1 M Na_2SO_4, 0.001 M H_2SO_4. *E*(tip)=+1.2 V; *E*(substrate)=−0.8 V. **b** Same as **a** but with copper-rich areas indicated for common reference. **c** Copper EDX map of same 80×80 μm area shown in **a** and **b**. **d** SECM image of the same 80×80 μm area after electrodeposition of small amount of polypyrrole. Solution: 0.01 M $K_3Fe(CN)_6$, 1 M Na_2SO_4. *E*(tip)=0.0 V, *E*(substrate)=+0.6 V. **e** Same as **d** but with reference points included from image **b**. **f** Carbon EDX map of same 80×80 μm area shown in other images

results of which are shown in Fig. 2d, e. Several areas of enhanced cathodic tip current are visible, attributable to sites of polymer nucleation. Positive correlation is seen between these areas and the carbon-rich areas shown in the EDX map of Fig. 2f. The edge of a particularly large area of deposition is clearly evident in the lower left-hand corner of both the SECM and EDX images. It is clear that the polymer nucleates on the aluminum matrix and not on the copper-rich areas. Polymer nucleation is seen adjacent to the copper particle indicated at point 2, and polymer growth can be seen encircling the copper particles indicated at points 3 and 6. Copper spots 4 and 5 and to a lesser extent spots 3 and 6 in Fig. 2b exhibit the lowest anodic activity in Fig. 2e.

Video microscopy of electrodeposition on a model alloy To further examine the role of copper-rich inclusions in the electrodeposition process, video microscopy experiments were carried out using the model alloy described in the experimental section above (a pure Al substrate with an embedded Cu wire). Voltammetric data and selected images from the potentiodynamic deposition of polypyrrole onto this model alloy from a deposition solution containing pyrrole, Tiron, sodium sulfate, and sulfuric acid are shown in Fig. 3. Image A, obtained at 0.0 V, shows the bare aluminum matrix with the lower half of the copper dot (wire) visible at the top of the image. The linear sweep voltammogram shows a large anodic peak with current onset just above 0 V. Image B shows a darkened copper dot at ca. 0.55 V, indicating that the first peak in the voltammogram results from oxidation of the copper and its subsequent passivation. Oxides of Cu are not stable under the acidic conditions of these experiments [31], but passivation due to formation of nonconducting $CuSO_4$ under acidic conditions is known [32], a result of $CuSO_4$ supersaturation near the Cu surface as Cu(II) is released into concentrated sulfate-containing electrolytes. (Close examination of the movie generated from this experiment clearly shows a physical transformation occurring on the Cu surface at potentials between 0.46 and 0.53 V, possibly corresponding to precipitation of $CuSO_4$ leading to passivation.)

Figure 3 shows a large anodic current increase again at potentials greater than 0.6 V, corresponding to nucleation and growth of the polymer. Image C, obtained at 0.81 V, shows that nucleation occurs over the entire aluminum matrix, but not on the passivated copper (note: the copper dot appears lighter in color due to the automatic contrast and brightness functions of the video camera; the actual appearance of the copper did not change following its oxidation). The full polymer layer shown at 1.28 V in image D indicates complete coverage of the aluminum matrix, but no polymer growth onto the copper—consistent with the SECM results shown above. This was true in most every trial of this experiment. Occasionally, polymer nucleation was observed on the copper surface, but this was very rare. When nucleation did occur on the copper, the number of nucleation sites was small, and almost no polymer growth occurred at these sites. Also on rare occasions, polymer growth was observed extending from the aluminum matrix over the outer edges of the copper.

The polymer nucleation and growth shown in Fig. 3c, d appeared to occur simultaneously over the entire aluminum matrix, even adjacent to the Cu dot. Under different conditions, however, nucleation was observed to occur preferentially at sites some distance away from the copper, with directional growth back toward the copper. This behavior can be seen quite clearly in Fig. 4, where the 1 M Na_2SO_4 and 0.001 M H_2SO_4 in the deposition solution were replaced by 1 M $NaNO_3$. The voltammogram in Fig. 4 shows marked differences to that of Fig. 3. Copper oxidation once again commences at 0.10 V; however, there is no isolated oxidation peak (i.e., no passivation) as in Fig. 3, and oxidation continues over a much larger potential range.

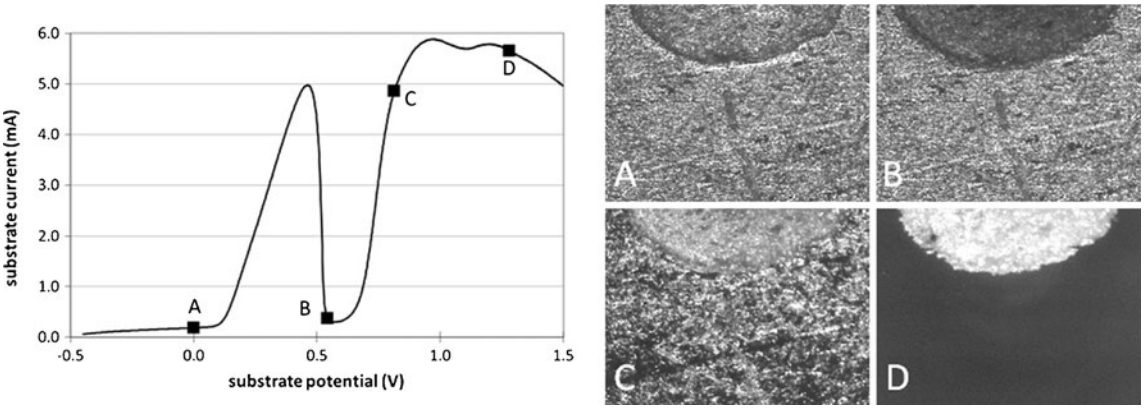

Fig. 3 *Left* Potentiodynamic electrodeposition voltammogram for polypyrrole on the model alloy (pure Al substrate with embedded 1-mm diameter copper wire). Deposition solution: 0.1 M pyrrole, 0.1 M Tiron, 1 M Na_2SO_4, 0.001 M H_2SO_4. Sweep rate, 10 mV/s. *Right* selected video microscopy images showing substrate during various stages of deposition. Images correspond to the indicated points on the voltammogram

Further observations have shown the presence of the isolated oxidation peak to be dependent on the sulfate concentration in the deposition solution. It is always present with 1 M Na_2SO_4, but not when the concentration drops to 0.1 M.

Figure 4 shows an increase in the slope of the anodic current at 0.60 V, signaling the beginning of electrodeposition and causing the potentiostat to quickly reach its current limit due to simultaneous mediated electrodeposition and copper oxidation. (This current limit is never observed with 1 M Na_2SO_4 present in the deposition solution since the copper is passivated by 0.60 V.) Images C and D show that polymer deposition follows an inward path toward the copper dot, and when the deposition is stopped at 1.5 V (image D) a small ring of bare aluminum is still visible surrounding the copper (again, despite the apparent change in appearance of the copper surface from image B to image C, the actual appearance was unchanged). Image C also shows a small portion of uncoated aluminum in the bottom right-hand corner, which is a portion of the substrate covered by the tape used to seal the sample in the cell; image D indicates that polymer growth extends to cover this region by 1.5 V.

The inward directional growth clearly observed with NO_3^- as the electrolyte in Fig. 4 was sometimes observed with SO_4^{2-} as well, although it was typically subtle and could only be seen during video playback by slowly scanning the individual images through a very small potential range. No indication of directional growth was ever observed when the experiments were repeated using a pure aluminum substrate (with no embedded copper wire), indicating that this phenomena is related to the presence of the copper within the aluminum matrix. We speculate that directional growth of polypyrrole in the absence of sulfate is the result of Cu(II) release from the copper dot, either from direct oxidation or from dissolution of an unstable oxide layer, the Cu(II) then diffusing radially outward from the copper dot. Since Tiron is a good complexing agent for a number of divalent and trivalent metal ions including Cu(II) [33, 34], its complexation with Cu(II) would effectively shut down the mediation mechanism within the diffusion field of the Cu(II), resulting in no deposition within this region. In the presence of a high sulfate concentration, however, these copper ions instead react to form $CuSO_4$, leaving the Tiron free for mediation of the polymer oxidation. Further support for this mechanism is the observation that, for galvanostatic electrodeposition at 1 mA/cm^2 (ca. 0.5 V), addition of the strong complexing ligand EDTA leads to polymer deposition right up to the edge of the copper dot (i.e., eliminates the directional growth on the Al matrix), presumably due to EDTA's stronger binding affinity for Cu(II), thereby releasing the Tiron and enabling the mediation mechanism.

To conclude, we suggest that passivation of Cu-rich sites on AA2024-T3 under conditions of high sulfate concentration (1 M) inhibits electron transfer activity at these sites, preventing polymer nucleation and deposition on the Cu sites. In the absence of Cu site passivation (at low sulfate concentration or in the absence of sulfate), continuous Cu ion release during polymer deposition would inhibit polymer nucleation on and near the Cu sites due to complexation of the mediator. Lateral (2D) growth of polymer would then be required to cover such areas.

Conclusions

While the copper-rich inclusions of AA2024-T3 demonstrate the highest electrochemical activity prior to electrodeposition of polymer, these sites do not maintain this activity during the electrodeposition process. Prior to deposition when the substrate is at the open-circuit potential, these sites are maintained in their active (non-oxidized) state. Upon application of a substrate potential sufficiently positive to

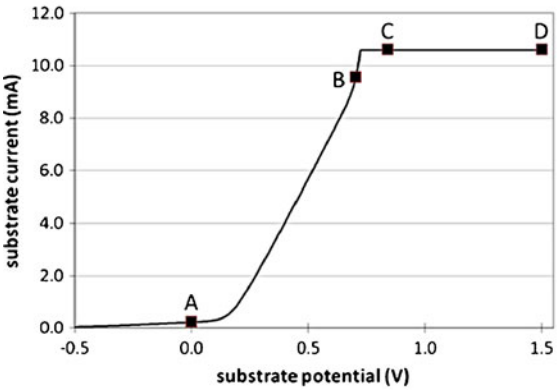

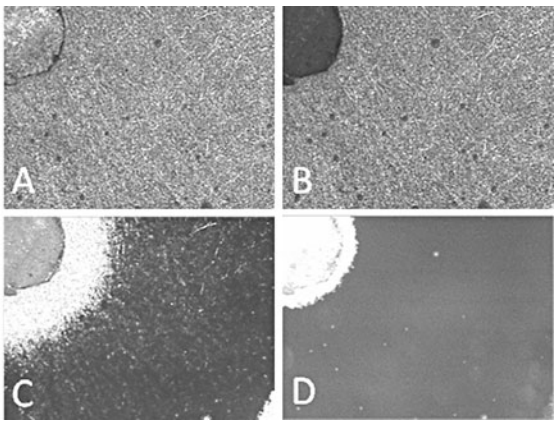

Fig. 4 *Left* Potentiodynamic electrodeposition voltammogram for polypyrrole on the model alloy. Deposition solution: 0.1 M pyrrole, 0.1 M Tiron, 1 M $NaNO_3$. Sweep rate, 10 mV/s. *Right* selected video microscopy images showing substrate during various stages of deposition. Images correspond to the indicated points on the voltammogram

initiate polymer nucleation and growth, these sites either passivate (e.g., at high concentration of sulfate) or undergo dissolution and release Cu ions that complex the mediator (Tiron) and thereby inhibit its oxidation and the mediation mechanism. Nucleation, therefore, is limited to sites on the aluminum matrix. Continued electrodeposition promotes lateral growth of the polymer from these nucleation sites and results in complete coverage of the substrate. These nucleation sites are most likely limited in number, although continued growth of the conducting polymer effectively increases the size of the active electrode for mediator oxidation and further deposition. At present, we do not know the nature of these nucleation sites on the aluminum matrix. Previous work from other laboratories [35, 36] as well as our own [14] has shown that both cathodically and anodically active sites can be identified on pure aluminum with SECM, and these sites have been attributed to structural and/or electronic defects in the native oxide. We speculate that these defect sites may be responsible for initiating nucleation of electrodeposited polymer, and experimental evidence establishing such a relationship is a goal of current work in our laboratory.

Acknowledgments We gratefully acknowledge support of this research by the Air Force Office of Scientific Research under grants FA9550-06-1-0461 and FA9550-07-1-0370 and by the Concordia Chemistry Research Endowment. We also thank Mr. Scott Payne of the NDSU Electron Microscopy Center for assistance with the SEM/EDX imaging.

References

1. Tallman DE, Bierwagen GP (2007) Corrosion protection using conducting polymers. In: Skotheim TA, Reynolds JR (eds) Handbook of conducting polymers, vol 2, 3rd edn. CRC, Boca Raton, pp 15/11–15/53
2. Zinger B (1988) Catalytic electrosynthesis of conducting polymers. J Electroanal Chem Interfacial Electrochem 244(1–2):115–121
3. Vang C, Dewald M, Richter A, Tallman DE, Wallace GG, Bierwagen GP (2002) Electrocatalytic polymerization of polypyrrole on Al 2024-T3 alloy. Polymer preprints. Am Chem Soc Div Polym Chem 43(1):742–743
4. Tallman DE, Vang C, Wallace GG, Bierwagen GP (2002) Direct electrodeposition of polypyrrole on aluminum and aluminum alloy by electron transfer mediation. J Electrochem Soc 149(3):C173–C179
5. Tallman DE, Vang CK, Dewald MP, Wallace GG, Bierwagen GP (2003) Electron transfer mediated deposition of conducting polymers on active metals. Synth Met 135–136:33–34
6. Tallman DE, Dewald MP, Vang CK, Wallace GG, Bierwagen GP (2004) Electrodeposition of conducting polymers on active metals by electron transfer mediation. Curr Appl Phys 4:137–140
7. Levine KL, Tallman DE, Bierwagen GP (2005) The mediated electrodeposition of polypyrrole on aluminium alloy. Aust J Chem 58(4):294–301
8. Parks GA (1965) The isoelectric points of solid oxides, solid hydroxides, and aqueous hydroxo complex systems. Chem Rev 65(2):177–198
9. Rocen JJ, Cerovic LS, Milonjic SK (2005) Adsorption of Tiron onto alumina. Mater Sci Forum 494:399–404
10. Gulicovski JJ, Cerovic LS, Milonjic SK (2008) Stability of alumina suspensions in the presence of Tiron. Ceram Int 34(1):23–26. doi:10.1016/j.ceramint.2006.07.010
11. Davis JR (1999) Corrosion of aluminum and aluminum alloys, 1st edn. ASM Int, Materials Park
12. Bard AJ, Mirkin MV (eds) (2001) Scanning electrochemical microscopy, vol 8. Monographs in electroanalytical chemistry and electrochemistry. Marcel Dekker, New York
13. Jensen MB, Bjordahl TJ, Tallman DE, Bierwagen GP (2007) Studies of electron transfer at aluminum alloy surfaces by scanning electrochemical microscopy. ECS Transactions 3:545–555
14. Jensen MB, Guerard A, Tallman DE, Bierwagen GP (2008) Studies of electron transfer at aluminum alloy surfaces by scanning electrochemical microscopy. J Electrochem Soc 155(7):C324–C332
15. Kwak J, Lee C, Bard AJ (1990) Scanning electrochemical microscopy. V. A study of the conductivity of a polypyrrole film. J Electrochem Soc 137(5):1481–1484
16. Arca M, Mirkin MV, Bard AJ (1995) Polymer films on electrodes. 26. Study of ion transport and electron transfer at polypyrrole films by scanning electrochemical microscopy. J Phys Chem 99 (14):5040–5050
17. Kapui I, Gyurcsanyi RE, Nagy G, Toth K, Arca M, Arca E (1998) Investigation of styrene-methacrylic acid block copolymer micelle doped polypyrrole films by scanning electrochemical microscopy. J Phys Chem B 102(49):9934–9939. doi:10.1021/jp982826h
18. Kranz C, Wittstock G, Wohlschlager H, Schuhmann W (1997) Imaging of microstructured biochemically active surfaces by means of scanning electrochemical microscopy. Electrochim Acta 42(20–22):3105–3111
19. Mandler D (2001) Micro- and nanopatterning using the scanning electrochemical microscope. In: Bard AJ, Mirkin MV (eds) Scanning electrochemical microscopy. Marcel Dekker, New York, pp 593–627
20. Marck C, Borgwarth K, Heinze J (2001) Generation of polythiophene micropatterns by scanning electrochemical microscopy. Chem Mater 13(3):747–752. doi:10.1021/cm001062r
21. Radtke V, Heinze J (2004) Scanning electrochemical microscopy as a versatile tool for modifying surfaces. Zeitschrift fuer Physikalische Chemie 218(1):103–121
22. Szunerits S, Knorr N, Calemczuk R, Livache T (2004) New approach to writing and simultaneous reading of micropatterns: combining surface plasmon resonance imaging with scanning electrochemical microscopy (SECM). Langmuir 20(21):9236–9241. doi:10.1021/la0492557
23. Evans SAG, Brakha K, Billon M, Mailley P, Denuault G (2005) Scanning electrochemical microscopy (SECM): localized glucose oxidase immobilization via the direct electrochemical microspotting of polypyrrole-biotin films. Electrochem Commun 7(2):135–140. doi:10.1016/j.elecom.2004.11.019
24. Fortin E, Mailley P, Lacroix L, Szunerits S (2006) Imaging of DNA hybridization on microscopic polypyrrole patterns using scanning electrochemical microscopy (SECM): the HRP biocatalyzed oxidation of 4-chloro-1-naphthol. Analyst 131 (2):186–193
25. Ghilane J, Martin P, Janin M, Randriamahazaka H, Hapiot P, Lacroix J-C (2009) Electrochemical investigation of thin PEDOT film above an insulating substrate using scanning electrochemical microscopy. Electrochem Commun 11(12):2304–2307. doi:10.1016/j.elecom.2009.10.017
26. Ghilane J, Martin P, Janin M, Randriamahazaka H, Hapiot P, Lacroix J-C (2010) Electrochemical investigation of thin PANI

film onto insulating substrate using scanning electrochemical microscopy. ECS Transactions 25:89–95
27. Naoi K, Takeda M, Kanno H, Sakakura M, Shimada A (2000) Simultaneous electrochemical formation of Al_2O_3/polypyrrole layers (I): effect of electrolyte anion in formation process. Electrochim Acta 45(20):3413–3421
28. Huelser P, Beck F (1990) Electrodeposition of polypyrrole layers on aluminum from aqueous electrolytes. J Appl Electrochem 20(4):596–605
29. Hagans PL, Haas CM (1994) Influence of metallurgy on the protective mechanism of chromium-based conversion coatings on aluminum–copper alloys. Surf Interface Anal 21(2):65–78
30. Buchheit RG, Grant RP, Hlava PF, McKenzie B, Zender GL (1997) Local dissolution phenomena associated with S phase (Al_2CuMg) particles in aluminum alloy 2024-T3. J Electrochem Soc 144(8):2621–2628
31. Jones DA (1996) Principles and prevention of corrosion, 2nd edn. Prentice Hall, Englewood Cliffs
32. Palaniappa M, Jayalakshmi M, Narasimhan BRV, Balasubramanian K (2008) Double step chronocoulometric studies on industrial copper alloy in acidic copper sulfate electrolytic solutions—part II. Int J Electrochem Sci 3(5):656–665
33. Kiss T, Sovago I, Martin RB (1989) Complexes of 3,4-dihydroxyphenyl derivatives. 9. Aluminum(3+) binding to catecholamines and tiron. J Am Chem Soc 111(10):3611–3614
34. Nepal JK, Dubey SN (1986) Thermodynamics of the complexation reactions of manganese(II), iron(II), cobalt(II), nickel (II), copper(II), and zinc(II) with 4-nitrocatechol and tiron. Indian J Chem Sect A Inorg Phys Theor Anal 25A(5):485–487
35. Serebrennikova I, White HS (2001) Scanning electrochemical microscopy of electroactive defect sites in the native oxide film on aluminum. Electrochem Solid State Lett 4(1):B4–B6
36. Serebrennikova I, Lee S, White HS (2002) Visualization and characterization of electroactive defects in the native oxide film on aluminum. Faraday Discussions 121:199–210